Switching Response of Dual-Output Mach-Zehnder Modulator in Channel-Interleaved Photonic Analog-to-Digital Converter

Lei Yu (于 磊), Weiwen Zou (邹卫文)*, Guang Yang (杨光), Xinwan Li (李新碗), and Jianping Chen (陈建平)

State Key Laboratory of Advanced Optical Communication Systems and Networks, Department of Electronic Engineering, Shanghai Jiao Tong University, Shanghai 200240, China

**Corresponding author: wzou@sjtu.edu.cn*

Received Month X, XXXX; accepted Month X, XXXX; posted online Month X, XXXX

This Letter theoretically and experimentally studies the response of photonic switching in a channel-interleaved photonic analog-to-digital converter (PADC) with high sampling rate and wide input frequency range. A figure of merit (FoM) is introduced to evaluate the switching response of the PADC when a dual-output Mach-Zehnder modulator (MZM) is served as the photonic switch to parallelize the sampled pulse train into two channels. After the optimization of the FoM and utilization of channel-mismatch compensation algorithm, the system bandwidth of PADC is expanded and the signal-to-distortion ratio (SDR) is enhanced.

OCIS Codes: 060.5625, 230.0250, 250.4745, 000.4430.
doi:10.3788/COLXXXXXX.XXXXXX.

The increasing demand for the processing of signal with high frequency and wide bandwidth in modern scientific research and engineering requires the signal acquisition technology with high sampling speed and high resolution [1-5]. There is a well-known electronic bottleneck of electronic analog-to-digital converters (EADCs), which is essentially limited by the timing jitter at the level of a hundred femtoseconds. Besides, the analog bandwidth of EADCs is only few gigahertz [6]. Thanks to the low timing jitter and broad bandwidth of photonics, photonic analog-to-digital converters (PADCs) [7, 8] offer an alternative solution to overcome the bottleneck faced by EADCs. The feasibility of PADC in breaking through the bandwidth limitation of EADC has been verified in radar systems [1-4].

Among several schemes of PADCs, photonic sampling and electronic quantizing ADC [7, 8] can achieve high sampling speed and high resolution. A stable mode locked laser (MLL) with low timing jitter [9, 10] serves as the sampling source, which guarantees a precise sampling time and a digitized signal with low jitter-limited noise floor. A photonic modulator with wide input frequency range is served as a photonic sampling gate to enlarge the analog input frequency range. In order to reduce the sampling speed as well as the input frequency range at the electronic backend, high-speed PADC systems ought to be demultiplexed into multiple channels [11-15]. To take advantage of the wide bandwidth of photonics, an array of photonic switches can be laid in front of the photo-diode (PD) array [16, 17] for photonic demultiplexing (i.e. channel interleaving). The electronic backend consists of an array of parallel EADCs with lower speed, narrower bandwidth, and higher precision, resulting in wide input frequency range and a high sampling speed which is the product of the sampling rate of a single EADC and the number of channels.

J. A. Bell *et al.* first demonstrated the photonic switch based channel-interleaved PADC system to obtain 2.8 bits ENOB (effective number of bits) with a sampling rate of 2 GS/s [17]. Later, a 505 MS/s channel-interleaved PADC system [8], which includes a 1-to-8 photonic switch, was reported with the maximum ENOB of 8.2 bits and a calibration technique [18] was developed for the suppression of channel mismatch distortion. Up to date, the laser sources utilized were mostly passively mode-locked lasers (PMLLs) [8, 16-18]. Due to the limited repetition rate of PMLLs, this scheme cannot simultaneously satisfy the requirements of high sampling speed and wide input frequency range. With the development of MLLs with higher repetition rate, we have recently investigated the pulse shape mismatch of the sampling clock in channel-interleaved PADC [15], which provides a flat frequency response within a wide input frequency range. However, the effect of the photonic switches on the channel-interleaved PADC has not been thoroughly studied.

In this Letter, we investigate theoretically and experimentally the switching response of the channel-interleaved PADC. Combined with the spectral analysis [7, 15], a figure-of-merit (FoM) that evaluates the effect of the photonic switch in the channel-interleaved PADC is defined and a numerical simulation of the impact of the FoM on the parameters of the photonic switch is performed. In the experiment, an actively mode locked laser (AMLL) with high repetition rate serves as the optical sampling clock and a dual-output Mach-Zehnder modulator (MZM) is used as the photonic switch. Under the optimization of the FoM, the pulse train of the AMLL is correspondingly demultiplexed into two channels by the dual-output MZM and the digitized data of the two channels is interleaved in the digital domain and reconstructed by the channel-mismatch compensation algorithm to suppress mismatch spurs.

The experimental setup of the channel-interleaved PADC is schematically plotted in Fig. 1. An AMLL (Calmar PSL-10-TT) is used as the optical sampling clock. A synthesizer (Keysight E8257D) outputs a microwave signal at 20 GHz, which is split into two paths. One path is used to seed the AMLL for the generation of a 20 GS/s optical sampling clock and the other is connected with a frequency divider (RF Bay FPS-2-20) to generate a 10 GHz driving signal. A band-pass filter (SinoSciTe FL2CX10CX02CL12) is used to suppress the harmonics of 10 GHz signal. The optical sampling clock is amplified by an optical amplifier (AMP, Calmar AMP-ST30) and passes through a Mach-Zehnder modulator

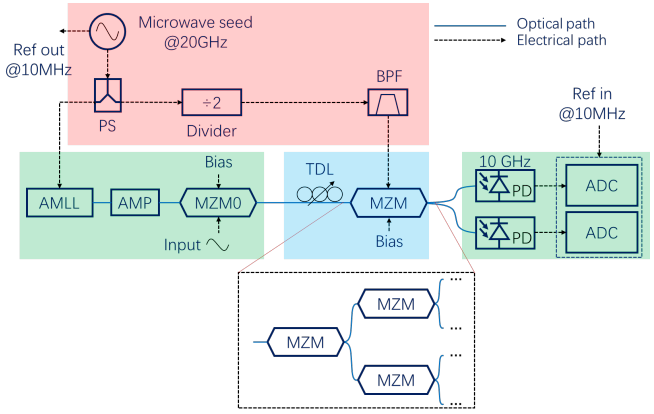

Fig. 1. Experimental setup of a channel-interleaved PADC with an AMLL for optical sampling clock and a dual-output MZM for photonic switch. AMLL: actively mode-locked laser, AMP: optical amplifier, MZM: Mach-Zehnder modulator, TDL: tunable delay line, PS: power splitter, BPF: band-pass filter, PD: photo-diodes, ADC: analog-to-digital converter.

(MZM0, Photoline MXIQ-LN-40) with 40 GHz analog input frequency range for photonic sampling. A microwave generator (Rhode & Schwarz SMA 100A) is used to generate the signal to be sampled. The 10 GHz driving signal is applied to drive the photonic switch. After photonic sampling, the sampled pulse train with the sampling rate of 20 GS/s is demultiplexed into two channels by a dual-output MZM (EOSpace AX-1x2-0MSS-20) which is served as a photonic switch. As shown in the dotted box in Fig. 1, the sampled pulse train can be easily expanded to multiple channels by a cluster of cascaded photonic switches (i.e. MZMs). In the digitizing of demultiplexed signals, two 10 GHz bandwidth PDs (Conquer PDA-10G-InGaAs-SM-FA) and two channels of a real-time oscilloscope (Keysight MSOS804A) are used. A 10-MHz reference output signal of the synthesizer (Keysight E8257D) is used as the reference clock of the oscilloscope during digitization.

The switching response of the MZM can be expressed by

$$\alpha(t)=\alpha_{\max}\frac{1}{2}\left(1-\frac{1}{\varepsilon}\right)\left(1+\eta\cos\left(\frac{\pi t}{T_S}\right)\right)+\frac{\alpha_{\max}}{\varepsilon}, \quad (1)$$

where $\alpha_{\max}$ is the maximum transmittance of the MZM based photonic switch and T_S is the temporal period of the optical sampling clock. $\varepsilon=\alpha_{\max}/\alpha_{\min}$ denotes the extinction ratio of the photonic switch with $\alpha_{\min}$ is the minimum transmittance of the MZM based photonic switch. The demultiplexing index of η is defined by

$$\eta=\sin\left(M\pi\cos\phi\right), \quad (2)$$

where ϕ is the phase offset between the sampled pulse train and the driving signal of MZM. $M=V_0/V_\pi$ is the modulation index where V_π is the half-wave voltage of the MZM and V_0 represents the amplitude of the driving signal to the MZM.

The transmission model of channel-interleaved PADC [7, 15] was investigated whereas the photonic demultiplexing process is simplified as an ideal pulse response. However, considering the switching response of MZM as described in Eq. (1), a more explicit model can be derived. The spectrum of digitized data in a demultiplexed channel can be correspondingly evaluated. Here, we define the ratio of the spectrum power of digitized data with and without the photonic demultiplexing, which is described by

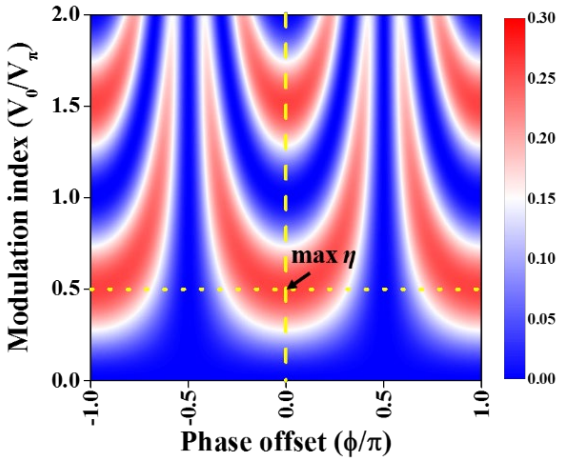

Fig. 2. Numerical simulation of the ratio of the spectrum power of digitized data with and without photonic demultiplexing as a function of the modulation index and phase offset.

$$\frac{P_{demux}}{P_{original}}=\alpha_{\max}^2\left(1-\frac{1}{\varepsilon}\right)^2\times\frac{\eta^2}{4} \quad (3)$$

where P_{demux} and P_{original} are the digitized signal power with and without the photonic demultiplexing, respectively. Note that the similar derivation can be applied to multiple channels with a cluster of cascaded MZMs (i.e. photonic switches).

Figure 2 shows the simulation result of the dependence of $P_{demux}/P_{original}$ on the amplitude (i.e. modulation index) and phase offset of the driving signal applied to the MZM. The input signal is set to be an 11-GHz single tone. It indicates that the ratio of signal amplitude varies periodically with the phase offset at the period of π. If there is a nonzero phase offset, the amplitude of the driving signal is increased to optimize the photonic switching response. When the phase of the driving signal perfectly matches with the optical sampling clock, the amplitude of the driving signal has a minimum value (0.5 V_π) for the maximum η, which depicts as the crossing point of the dotted and dash lines in Fig. 2. When the phase mismatch is $\pi/2$, there is no switching response and the parallelization is disabled. Since the extinction ratio and the maximum transmittance (i.e. ε and $\alpha_{\max}$) are given for a specific MZM, the demultiplexing index of η is the FoM of the photonic switch in the PADC system. By manipulation of both amplitude and phase offset of the driving signal of the MZM, the photonic switching response determined by the FoM [see Eq. (3)] can be correspondingly optimized.

Note that the phase offset ϕ can be implemented by tuning the phase of the driving signal or optimizing the time delay of sampled pulse train. In the experiment, an optical tunable time delay line (TDL: General Photonics MDL-002) is inserted before the MZM to precisely adjust the phase offset ϕ. The bias voltage applied to the dual-output MZM is set at the quadrature bias point. Figures 3(a) and 3(b) depict the power of the digitized data at 11 GHz under different driving powers and phase offset ϕ of the driving signal to the MZM. Since V_π of the MZM is about 6.4 V and the impedance is 50 Ω, the power of the driving signal is set to ~20 dBm to achieve a modulation index of 0.5. According to Eq. (3), the demultiplexing index η is calculated. The digitized power is depicted in Fig. 3(a) or Fig. 3(b) as a function of the RF power (when the phase offset is set to 0) or phase offset (when the RF amplitude is set to $V_\pi/2$) of the driving signal, respectively. Note that both the digitized power

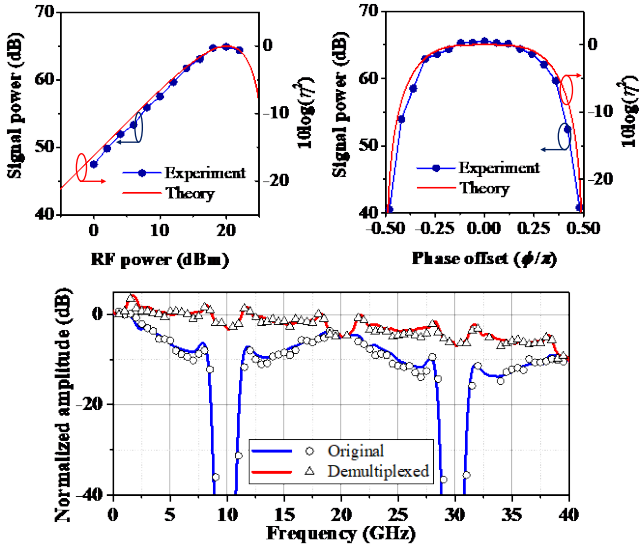

Fig. 3. Measured power of the digitized data and the FoM (η) with different powers (a) and phase offsets (b) of the driving signal to the dual-output MZM. The symbols denote the experimentally measured data and the solid curves represent the simulated results. (c) Microwave response of the PADC with and without the photonic demultiplexing.

and the calculated η are plotted in the dB scale. They are in good agreement with the simulated results except for a constant offset, indicating the validation of the theoretical analysis of Eq. (3). When the 10 GHz microwave signal driving the dual-output MZM is turned off, the digitized data represents the experimental results of the PADC without the photonic demultiplexing, the sampling rate of the oscilloscope is set to 20 GS/s to match the one-channel system without demultiplexing. Figure 3(c) summarizes the measured microwave responses of the PADC with and without the photonic demultiplexing. Due to the limited bandwidth of the oscilloscope of ~8.4 GHz, which is lower than the Nyquist bandwidth of 10 GHz of the PADC without the photonic

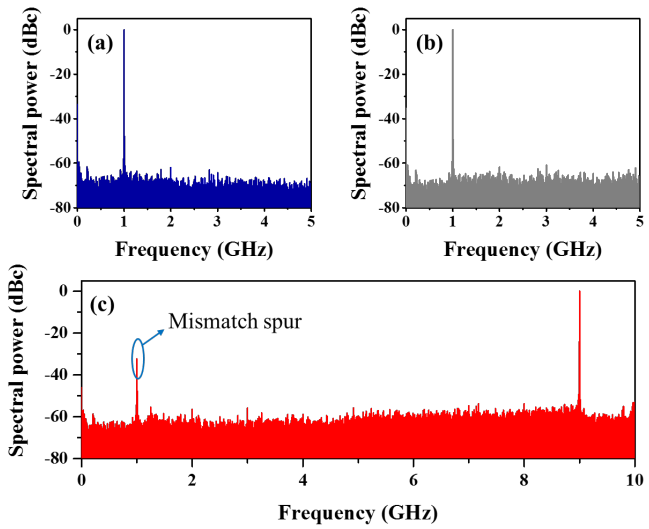

Fig. 4. (a) and (b) FFT spectra of the digitized data of 11 GHz single tone input signal in two demultiplexed channels, respectively. (c) FFT spectrum of the data reconstructed via the time-interleaving of two channels.

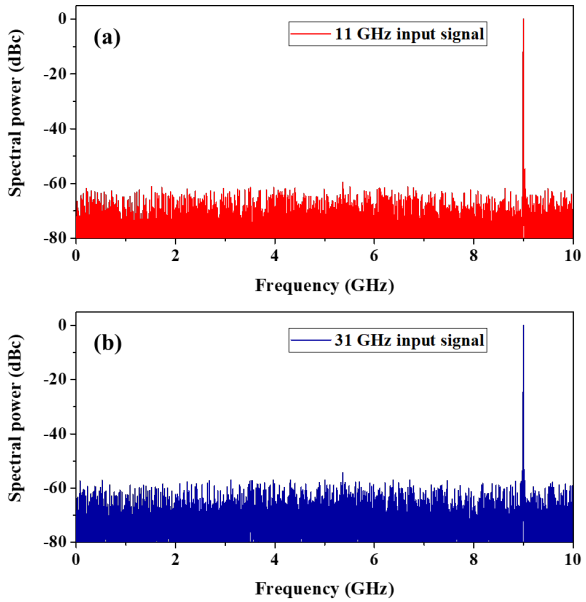

Fig. 5. FFT spectra of the reconstructed data after mismatch compensation when the frequency of the input signal to be sampled is 11 GHz and 31 GHz, respectively.

demultiplexing, there are two notches near 10 GHz and 30 GHz. However, the notches are significantly recovered because the Nyquist bandwidth of the two-channel interleaved PADC is reduced to 5 GHz for each channel. As a result, the input frequency range of PADC system can be expanded and it is possible to get close to the bandwidth of the MZM0 (40 GHz) under the subsampling principle.

In order to verify the feasibility of sampling in the PADC, an 11-GHz single tone with the power of 6 dBm is applied to the MZM0. Note that the sampling rate of each demultiplexed channel is 10 GS/s and thus the sampling rate of each channel in the oscilloscope is correspondingly preset to be 10 GS/s, and the digitized spectrum of 11 GHz input signal is folded to 1 GHz according to the sub-sampling principle [13]. The spectra of the digitized data in two demultiplexed channels are depicted in Fig. 4(a) and Fig. 4(b), respectively. The high-order distortions are suppressed by optimizing the bias voltage of the MZM0. The SDR of the two channels in Fig. 4(a) and 4(b) are 59.3 dBc and 60.5 dBc.

The data in two channels are time-interleaved to reconstruct the digitized data. The sampling rate turns to be 20 GS/s after time-interleaving, which folds the 11 GHz input signal back to 9 GHz. The corresponding spectrum is illustrated in Fig. 4(c). Due to the mismatches in the amplitude and phase offset of two channels, there are mismatch spurs appearing in the spectrum of the reconstructed data, leading to an SDR of 32.3 dBc. In order to suppress the spurs, a channel-mismatch compensation algorithm [7] is applied to the digitized data. After the channel-mismatch compensation, the spectrum of digitized data of the 11 GHz signal is depicted in Fig. 5(a). The corresponding SDR is increased to 54.9 dBc, which reaches the maximum value of the EADC and corresponds to an ENOB of 6.9 bits according to the definition [7]. Furthermore, a 31 GHz input signal is also preceded by the same method. The spectrum of the reconstructed data after mismatch compensation is also illustrated in Fig. 5(b). Note that the FFT spectrum of the digitized data is also folded to 9 GHz due to the sub-sampling principle. The SDR is 51.7 dBc and the corresponding ENOB is 6.1 bits.

In conclusion, the influence of photonic switch on channel-interleaved PADC system is theoretically and experimentally investigated. The FoM of the photonic switch based demultiplexing is extracted according to the theoretical analysis. A dual-output MZM is used as the photonic switch and two demultiplexed channels are digitized in each channel with the optimized FoM. After the data reconstruction and channel-mismatch compensation, the SDRs of the digitized 11 GHz and 31 GHz signal are significantly improved and the input frequency range of PADC system is correspondingly broadened.

This work was partially supported by National Natural Science Foundation of China (grant no. 61822508, 61571292 and 61535006).

References

1. P. Ghelfi, F. Laghezza, F. Scotti, G. Serafino, A. Capria, S. Pinna, D. Onori, C. Porzi, M. Scaffardi, A. Malacarne, V. Vercesi, E. Lazzeri, and A. Bogoni, Nature, **507**, 341 (2014).
2. W. Zou, H. Zhang, X. Long, S. Zhang, Y. Cui, and J. Chen, Scientific Reports, **6**, 19786 (2016).
3. S. Xu, W. Zou, G. Yang, and J. Chen, Chin. Opt. Lett. **16**, 062801 (2018).
4. J. Yang, S. Li, X. Xiao, D. Wu, X. Xue, and X. Zheng, Chin. Opt. Lett. **16**, 060605 (2018).
5. F. Scotti, F. Laghezza, S. Pinna, P. Ghelfi, and A. Bogoni, In OptoElectronics and Communications Conference and Photonics in Switching, Optical Society of America, 2013, paper TuO1_3.
6. H. Wei, P. Zhang, B. D. Sahoo, and B. Razavi, IEEE J. Solid-State Circuits, **49**, 1751 (2014).
7. G. Yang, W. Zou, L. Yu, K. Wu, and J. Chen, Opt. Express, **24**, 24061 (2016).
8. P. W. Juodawlkis, J. C. Twichell, G. E. Betts, J. J. Hargreaves, R. D. Younger, J. L. Wasserman, F. J. O'Donnell, K. G. Ray, and R. C. Williamson, IEEE Trans. Microw. Theroy Tech., **49**, 1840 (2001).
9. X. Li, W. Zou, and J. Chen, Opt. Lett., **39**(6), 1553 (2014).
10. J. Kim, S. Choi, W. Kim, B. Kang, W. Cho, G. Kim, and F. Rotermund, Chin. Opt. Lett., **16**, 061404 (2018).
11. T. R. Clark, J. U. Kang, and R. D. Esman, IEEE Photon. Technol. Lett., **11**, 1168 (1999).
12. R. Williamson, P. Juodawlkis, J. Wasserman, G. Betts, and J. Twichell, J. Lightwave Technol., **19**, 230 (2001).
13. J. Kim, M. J. Park, M. H. Perrott, and F. X. Kärtner, Opt. Express, **16**, 16509 (2008).
14. H. Zhang, W. Zou, G. Yang, and J. Chen, Chin. Opt. Lett., **14**, 030602 (2016).
15. G. Yang, W. Zou, L. Yu, and J. Chen, Opt. Lett., **43**, 3530 (2018).
16. F. Laghezza, F. Scotti, P. Ghelfi, A. Bogoni, and S. Pinna, In Radar Conference (RADAR 2013), IEEE pp. 1-5.
17. J. A. Bell, M. C. Hamilton, and D. A. Leep, Proc. SPIE, **1562**, 276 (1991).
18. R. C. Williamson, R. D. Younger, P. W. Juodawlkis, J. J.Hargreaves, J. C. Twichell, In 2003 Digest of the LEOS Summer Topical Meetings, 2003, paper MC4.2/22-MC4.2/23.

1. P. Ghelfi, F. Laghezza, F. Scotti, G. Serafino, A. Capria, S. Pinna, D. Onori, C. Porzi, M. Scaffardi, A. Malacarne, V. Vercesi, E. Lazzeri, and A. Bogoni, "A fully photonics-based coherent radar system," Nature, **507**, 341 (2014).
2. W. Zou, H. Zhang, X. Long, S. Zhang, Y. Cui, and J. Chen, "All-optical central-frequency-programmable and bandwidth-tailorable radar," Scientific Reports, **6**, 19786 (2016).
3. S. Xu, W. Zou, G. Yang, and J. Chen, "Ultra-high range resolution demonstration of a photonics-based microwave radar using a high-repetition-rate mode-locked fiber laser," Chin. Opt. Lett. **16**, 062801 (2018).
4. J. Yang, S. Li, X. Xiao, D. Wu, X. Xue, and X. Zheng, "Broadband photonic ADC for microwave photonics-based radar receiver," Chin. Opt. Lett. **16**, 060605 (2018).
5. F. Scotti, F. Laghezza, S. Pinna, P. Ghelfi, and A. Bogoni,. "High precision photonic ADC with four time-domain-demultiplexed interleaved channels," In OptoElectronics and Communications Conference and Photonics in Switching, Optical Society of America, 2013, paper TuO1_3.
6. H. Wei, P. Zhang, B. D. Sahoo, and B. Razavi, "An 8 bit 4 GS/s 120 mW CMOS ADC," IEEE J. Solid-State Circuits, **49**, 1751 (2014).
7. G. Yang, W. Zou, L. Yu, K. Wu, and J. Chen, "Compensation of multi-channel mismatches in high-speed high-resolution photonic analog-to-digital converter," Opt. Express, **24**, 24061 (2016).
8. P. W. Juodawlkis, J. C. Twichell, G. E. Betts, J. J. Hargreaves, R. D. Younger, J. L. Wasserman, F. J. O'Donnell, K. G. Ray, and R. C. Williamson, "Optically sampled analog-to-digital converters," IEEE Trans. Microw. Theroy Tech., **49**, 1840 (2001).
9. X. Li, W. Zou, and J. Chen, "41.9 fs hybridly mode-locked Er-doped fiber laser at 212 MHz repetition rate," Opt. Lett., **39**, 1553 (2014).
10. J. Kim, S. Choi, W. Kim, B. Kang, W. Cho, G. Kim, and F. Rotermund, "550 MHz carbon nanotube mode-locked femtosecond Cr:YAG laser," Chin. Opt. Lett., **16**, 061404 (2018).
11. T. R. Clark, J. U. Kang, and R. D. Esman, "Performance of a time- and wavelength-interleaved photonic sampler for analog-digital conversion," IEEE Photon. Technol. Lett., **11**, 1168 (1999).
12. R. Williamson, P. Juodawlkis, J. Wasserman, G. Betts, and J. Twichell, "Effects of crosstalk in demultiplexers for photonic analog-to-digital converters," J. Lightwave Technol., **19**, 230 (2001).
13. J. Kim, M. J. Park, M. H. Perrott, and F. X. Kärtner, "Photonic subsampling analog-to-digital conversion of microwave signals at 40-GHz with higher than 7-ENOB resolution," Opt. Express, **16**, 16509 (2008).
14. H. Zhang, W. Zou, G. Yang, and J. Chen, "Dual-output modulation in time-wavelength interleaved photonic analog-to-digital converter based on actively mode-locked laser," Chin. Opt. Lett., **14**, 030602 (2016).
15. G. Yang, W. Zou, L. Yu, and J. Chen, "Influence of the sampling clock pulse shape mismatch on channel-interleaved photonic analog-to-digital conversion," Opt. Lett., **43**, 3530 (2018).
16. F. Laghezza, F. Scotti, P. Ghelfi, A. Bogoni, and S. Pinna, "Jitter-limited photonic analog-to-digital converter with 7 effective bits for wideband radar applications," In Radar Conference (RADAR 2013), IEEE pp. 1-5.
17. J. A. Bell, M. C. Hamilton, and D. A. Leep, "Optical sampling and demultiplexing applied to A/D conversion," Proc. SPIE, **1562**, 276 (1991).
18. R. C. Williamson, R. D. Younger, P. W. Juodawlkis, J. J.Hargreaves, J. C. Twichell, "Precision calibration of an optically sampled analog-to-digital converter," In 2003 Digest of the LEOS Summer Topical Meetings, 2003, paper MC4.2/22-MC4.2/23.